APL Materials

Alloying effects on superionic conductivity in lithium indium halides for all-solid-state batteries

Cite as: APL Mater. 6, 047903 (2018); https://doi.org/10.1063/1.5011378
Submitted: 31 October 2017 . Accepted: 08 February 2018 . Published Online: 26 February 2018

Alysia Zevgolis, Brandon C. Wood, Zerina Mehmedović, Alex T. Hall, Thomaz C. Alves, and Nicole Adelstein

Alloying effects on superionic conductivity in lithium indium halides for all-solid-state batteries

Alysia Zevgolis,[1,2] Brandon C. Wood,[3] Zerina Mehmedović,[2]
Alex T. Hall,[2] Thomaz C. Alves,[2] and Nicole Adelstein[2]
[1]*Georgetown University, Georgetown, District of Columbia 20057, USA*
[2]*San Francisco State University, San Francisco, California 94132, USA*
[3]*Lawrence Livermore National Laboratory, Livermore, California 94550, USA*

(Received 31 October 2017; accepted 8 February 2018; published online 26 February 2018; corrected 18 September 2018)

Alloying of anions is a promising engineering strategy for tuning ionic conductivity in halide-based inorganic solid electrolytes. We explain the alloying effects in $Li_3InBr_{6-x}Cl_x$, in terms of strain, chemistry, and microstructure, using first-principles molecular dynamics simulations and electronic structure analysis. We find that strain and bond chemistry can be tuned through alloying and affect the activation energy and maximum diffusivity coefficient. The similar conductivities of the $x = 3$ and $x = 6$ compositions can be understood by assuming that the alloy separates into Br-rich and Cl-rich regions. Phase-separation increases diffusivity at the interface and in the expanded Cl-region, suggesting microstructure effects are critical. Similarities with other halide superionic conductors are highlighted.
https://doi.org/10.1063/1.5011378

The search for solid-state electrolytes to enable all-solid-state batteries has yielded a number of candidates based on halide anions.[1–6] Unfortunately, none of these have been realized commercially, lacking stability to electrodes and voltage or room temperature conductivity matching liquid electrolytes, around 10^{-1} S/cm.[7] One approach to improving electrolytes is anion alloying. Among superionic conductors, this effect has been demonstrated in the antiperovskites and their analogs,[5,6,8] argyrodites,[9] and silver halides,[1,10,11] though the effects are often complex or not well described. Indeed, the most conductive alloy composition is difficult to predict since the potential effects of alloying are many. Factors such as strain, local composition gradients, and differences in local Li-anion bonding character may be relevant. The role of microstructure must also be considered since phase-separating versus solid solution forming systems can alter materials' properties in fundamentally different ways.

This letter explores alloying effects on the superionic conductivity of lithium indium halides, $Li_3InBr_{6-x}Cl_x$, with general implications for other halide alloys. The experimental measurement of conductivities has shown that alloying in $Li_3InBr_{6-x}Cl_x$ results in a non-monotonic trend, making the material an interesting case study. In particular, the $x = 0$ and $x = 3$ compositions have almost the same conductivity between 300 and 500 K (10^{-3} S cm^{-1} at 360 K), while $x = 2$ has significantly lower conductivity.[12]

Using first-principles molecular dynamics (MD) simulations, we identify the effect of alloying by simulating four compositions: $x = 0$ (Br_6), $x = 2$ (Br_4), $x = 3$ (Br_3), and $x = 6$ (Cl_6), where a shorthand for each composition is given in parenthesis. Among other tools, we leverage our novel bond character analysis, which we recently showed can distinguish between ionic (Coulombic) and polar-covalent character in the Li-halide bond.[13] This analysis gives significant additional insight into the chemical effect of alloying. The effect of phase separation is also considered, where strain leads to local concentration gradients that affect ionic conductivity. We find that these chemical, structural, and compositional factors are able to explain the non-monotonic trend in conductivities: Br_6–Br_3–Br_4–Cl_6 from highest to lowest.

Superionic diffusivity is due to a small activation energy barrier, E_a, and a large maximum diffusion coefficient, D_0, through the Arrhenius expression, $D = D_0 e^{\frac{-E_a}{k_B T}}$, where k_B is Boltzmann's constant and T is the temperature. Our study of $Li_3InBr_{6-x}Cl_x$ shows that it is necessary to computationally screen for new superionic electrolytes using both E_a and D_0. For example, Cl_6 has a smaller E_a than Br_3, but Br_3 has a larger diffusivity at 500 K, due to its larger D_0.

Børn–Oppenheimer[14] MD were run on $Li_3InBr_{6-x}Cl_x$ using the Quantum ESPRESSO plane-wave density functional theory (DFT) code.[15] Using the Nernst–Einstein relationship, the diffusion coefficients, D, were calculated. Figure 1 shows example Br_3 supercells with the Li-ions removed and an ordered indium (purple) sublattice. A time step of 20 a.u. (0.97 fs) and wavefunction and charge density cutoffs of 30 Ry and 300 Ry were used after convergence tests were run. Ultrasoft pseudopotentials[16] for Li, In, Cl, and Br were employed with the Perdew-Burke-Ernzerhof (PBE) exchange-correlation functional.[17] The pseudopotentials are Li.pbe-s-van_ak.UPF, In.pbe-d-rrkjus.UPF, Cl.pbe-n-van.UPF, and Br.pbe-van_mit.UPF.

We independently vary the composition, volume, and microstructure in the MD to isolate the effects of strain and chemistry. The four compositions were simulated as solid solutions with a random placement of Br and Cl in the supercell. For each alloy, the configurational complexity is too great to calculate the full ensemble. Thus, we optimize the geometry of 3–6 reference configurations and simulate the one with the lowest DFT ground state energy. The spread in energies, given in the supplementary material (Table SI.6), is at most 36 meV/atom, within the magnitude of thermal fluctuations at our simulation temperatures. The volumes for Br_6 (4389 Å^3) and Cl_6 (3638 Å^3) were optimized, and the Br_3 (4112 Å^3) and Br_4 (4262 Å^3) computational volumes were scaled according to the experimental trend in volume versus composition (Fig. 6). The alloyed compositions were simulated at three volumes: 4389, 4262, and 4112 Å^3. The computational lattice vectors for each supercell are given in Table SI.1 of the supplementary material. In addition, a nanophase (NP) separated supercell with a Cl-rich side and Br-rich side was simulated for the Br_3 composition (right cell in Fig. 1).

All compositions were simulated at multiple temperatures between 500 and 900 K to obtain E_a and D_0. MD simulations are equilibrated at temperature and then run for at least 25 ps. Across all compositions and volumes, except Cl_6, we see the non-Arrhenius behavior, consistent with our previous study on Li_3InBr_6.[13] The non-Arrhenius behavior indicates a change in diffusion mechanism and a variable E_a. The change in E_a does not occur at the same temperature for all compositions but often occurs between 800 K and 900 K (see Fig. SI.1 of the supplementary material). Thus, we report E_a between 500 and 800 K in Fig. 2.

Effect of volume and chemistry: The conventional paradigm of ionic conductivity suggests that diffusivity will increase as volume increases, but for the alloyed systems, the effect is much more profound. Diffusivity in $Li_3InBr_{6-x}Cl_x$ does not systematically increase with increasing volume because E_a does not systematically decrease. Figure 2(b) shows that Br_3 at the central 4262 Å^3 volume (yellow) has the highest E_a of that alloy computation, for example. The trend in D can only be understood by also considering the trends in D_0. The largest D_0 for the Br_3 and Br_4 alloys occurs at the ~3% expanded volumes [blue for Br_4 and yellow for Br_3 in Fig. 2(c)]. The far more subtle trend

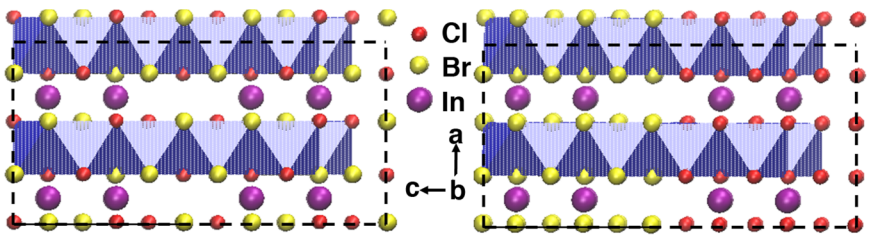

FIG. 1. $2 \times 2 \times 2$ supercell of $Li_3InBr_3Cl_3$. Blue octahedrons represent Li bound to six halides. Cl, Br, and In are shown as red, yellow, and purple. Black dashed lines indicate the "c-a" plane. The solid solution has a random placement of Cl and Br (left), whereas the nanophase separated microstructure alternates Cl and Br (right).

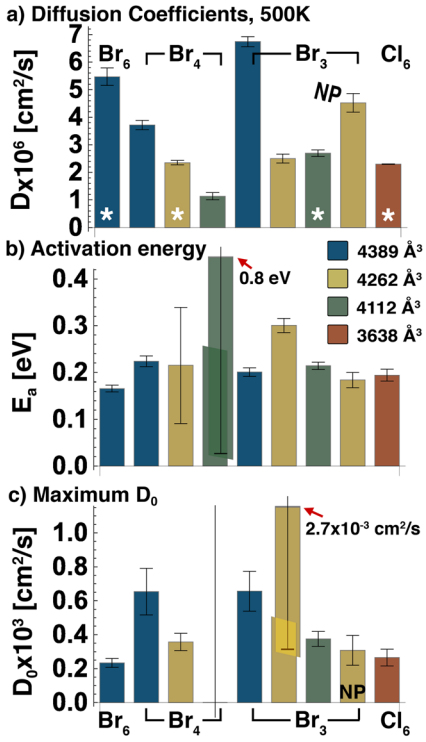

FIG. 2. Diffusion coefficients, $D \times 10^6$ cm^2/s at 500 K, maximum diffusion coefficients, $D_0 \times 10^3$ cm^2/s, and E_a in eV. The white star denotes the computational volume.

in E_a, which is a convolution of the size of the octahedral local minima and the tetrahedral transition state, is explored in the supplementary material.

D_0 characterizes the shape of the local minimum energy wells (curvature), which we probe by considering the effects of volume and chemistry. We posit that large values of D_0 are due to an "ideal" bond length that causes maximum bond frustration, increasing the jump attempt frequency. If Li^+ only had purely ionic bonds, it would sit in the center of the halide octahedra and bonds would have no strict angular preferences. In contrast, we previously showed that in Li_3InBr_6, many Li–Br bonds have polar-covalent character, with a narrower-than expected distribution of angles and shortened bond distances.[13] Polar-covalent bonds were rigorously defined via distance cutoffs and angle cutoffs based on the centers of Maximally Localized Wannier Functions (MLWF).[18] In this work, we adopt the same definition and analysis to classify bonds as containing chiefly polar-covalent or chiefly ionic character. Further details on the selection of cutoff criteria can be found in the supplementary material (Figs. SI.1 and SI.2), as well as in Ref. 13.

Bonds in lithium indium halide exhibit frustration in the inability of Li to form simultaneous polar-covalent bonds with all the halides in the octahedral site, which we previously discovered contributes to fast diffusion in Br_6.[13] The octahedral site is too large in Br_6, so each Br only has 1–2 simultaneous polar-covalent bonds. Since we no longer consider Li or the halides to be purely ionic, we stop including the charge superscripts.

The ability of Li to form simultaneous polar-covalent bonds depends on the size of the octahedral site, which can be characterized by the distance r_{X-c} from a halide (X) to the centroid of the site (c) in the relaxed supercell (Fig. 3). The distance from Li to the centroid r_{Li-c} depends on the cell volume and the Br/Cl composition; on average, r_{Li-c} is nonzero because of the oscillatory motion and a strong polar-covalent interaction, as described in our previous work.[13] We compute r_{Li-c} by extracting the Li-halide distance, r_{Li-X}, from the Li-X pair correlation function and subtracting r_{X-c}. We report r_{Li-c}/r_{X-c} in Fig. 3 and note the increasing trend with volume, contrary to what is expected from purely ionic bonds. At large volumes, Li interacts primarily with one halide, is far from the centroid, and cannot be easily captured in a polar-covalent bond by other halides in the octahedral site, which

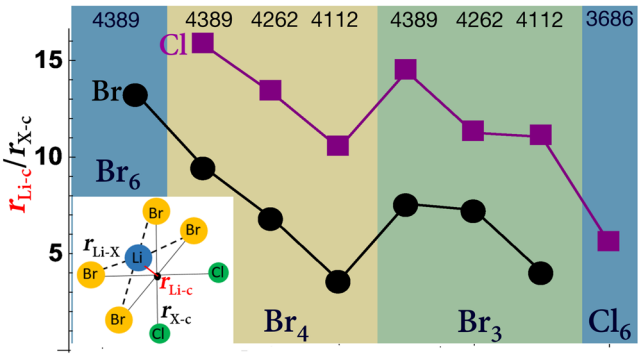

FIG. 3. The ratio of the Li-centroid distance ($r_{\mathrm{Li-c}}$) to the halide-centroid distance ($r_{\mathrm{X-c}}$) shows that Li stays close to the halide as the volume (in Å^3) increases. Purple is for X = Cl, and black is for X = Br. Inset: cartoon of Li close to Br neighbors and the Li-centroid distance indicated with the red line.

affects the jump attempt frequency and thus D_0. We point out that similar behavior was observed in $AgBr_xI_{1-x}$ alloys, for which silver-halide distances were maintained across large composition regions while distances to the site centroids increased with decreasing x.[19]

The Goldilocks effect is observed. If the Li-centroid is too large, Li cannot form simultaneous polar-covalent bonds. If the Li-centroid is too small, Li can form many simultaneous polar-covalent bonds easily. In these extreme simulations, frustration is reduced. The "just right" octahedral size leads to the largest D_0 values for each alloy: Br_4 with a volume of 4389 Å^3 and Br_3 with a volume of 4262 Å^3 [Fig. 2(c)]. While Br_3 with a volume of 4389 Å^3 also seems to have an intermediate Li-centroid distance, it is reasonable to expect that the octahedral site is too large using the Br_6 volume with a Br_3 composition; this D_0 has an intermediate value of 6.6×10^{-4} cm^2/s. The D_0 value of the Br_4 alloy at the small 4112 Å^3 volume could not be easily calculated because the data were severely non-Arrhenius over the range 500-800 K (see the supplementary material), so it is not provided in Fig. 2.

We count the number of polar-covalent bonds that an anion has, on average, for each volume and report the polar-covalent bonds as a percentage of total neighbors in Fig. 4. The general trends in polar-covalent bond character in the alloys are in accord with Fajan's rules, which state that Br–Li bonds are more polar-covalent than Cl–Li bonds.[20]

We get essential information about the polar-covalent bond strength by examining the effect of the temperature on polar-covalent bonds for Br_3. If polar-covalent bonds are competing, simultaneous

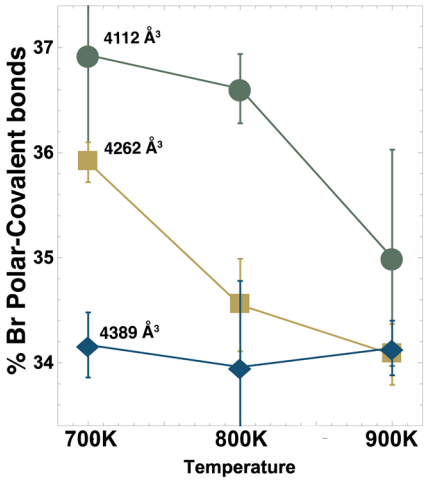

FIG. 4. Percentage of polar-covalent bonds around Br for Br_3. The error bars are calculated from the bootstrap sampling method (described in the supplementary material along with a sensitivity analysis).

bonds are tenuous and increasing the temperature can break the bonds. Figure 4 shows a significant change in the number of polar-covalent between 700 and 900 K for the 4262 Å^3 volume, which has the most frustrated Li–Br bonds. Increasing the temperature between 700 and 800 K breaks many of the polar-covalent bonds and helps explain the high D_0. In contrast, the small Br_3 cell has a larger percentage of polar-covalent bonds, which decreases significantly only at 900 K. The large Br_3 cell has a small and constant percentage of polar-covalent bonds. A similar steep trend (not shown) occurs in Br_4 with the 4389 Å^3 volume, which has the highest D_0 for that composition. The trends shown in Fig. 4 are robust with respect to changing the cutoffs defining ionic versus polar-covalent bonds, as described in the supplementary material. Highly frustrated bonds affect D_0 and E_a, contributing to the non-Arrhenius behavior. While frustration in the octahedral site affects E_a, variations in E_a are more tied directly to the volume of the tetrahedral site, as discussed in the supplementary material.

We find polar-covalent bonds forming at 2.9 Å and 2.65 Å for Li–Br and Li–Cl, respectively, regardless of composition (Figs. SI.1 and SI.2 of the supplementary material). Thus, Li has to be much closer to Cl than Br to form a bond with polar-covalent character. It follows that more Br neighbors lead to increased competition between polar-covalent bonds, which we previously showed to increase the jump rate in Li_3InBr_6.[13]

At the $x = 3$ composition, most Li ions have 3 Br neighbors. If we define $\Pi(\mathrm{Br} > 3)$ as the percentage of Li with an excess (>3) of Br neighbors, then the average value of $\Pi_{\mathrm{ave}}(\mathrm{Br} > 3) = 1.8\%$. However, if we consider only jumping Li, then $\Pi_{\mathrm{jump}}(\mathrm{Br} > 3) > \Pi_{\mathrm{ave}}(\mathrm{Br} > 3)$ indicates that excess Br neighbors lead to more jumps. This is seen in Fig. 5 which shows $\Pi_{\mathrm{jump}}(\mathrm{Br} > 3) - \Pi_{\mathrm{ave}}(\mathrm{Br} > 3)$ as a function of temperature and volume. For instance, at 500 K and with a 4112 Å^3 volume, the likelihood for having excess Br neighbors grows for jumping Li by 11.5% in absolute terms. As the temperature or volume increases, the effect of excess Br neighbors decreases because the frustration (competition) between these Li-Br bonds diminishes. Indeed, there is building consensus that frustration, the inability for a system with mobile ions to settle in a significantly deep energy minimum, affects superionic conductivity.[9,13,21–23] Frustrated bonds can set up a chain of correlated diffusion events, further increasing conductivity.

Effect of phase separation: Slightly expanded octahedral sites lead to a higher D_0. However, strain can also be induced by a phase separation of Br-rich and Cl-rich regions, either globally or at the nanoscale. We find that the trend in conductivity with alloying[12] is understood by assuming a nanophase (NP) microstructure for the Br_3 composition, which can be directly simulated (Fig. 1).

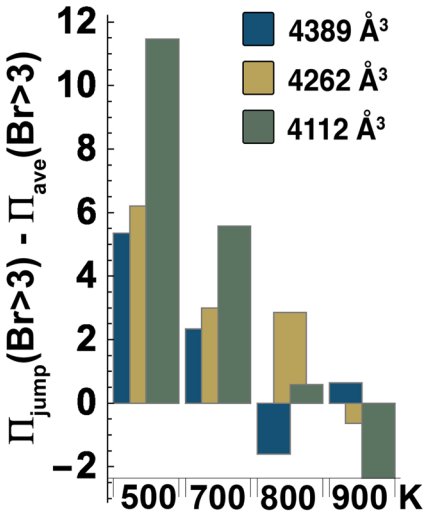

FIG. 5. $\Pi_i(\mathrm{Br} > 3)$ is the percentage of Li with Br neighbors >3, which leads to more jumps at small volumes and lower temperatures. $\Pi_{\mathrm{jump}}(\mathrm{Br} > 3) - \Pi_{\mathrm{ave}}(\mathrm{Br} > 3) > 0$ indicates that jumping Li ions are more likely to have excess Br neighbors (Br > 3) than average.

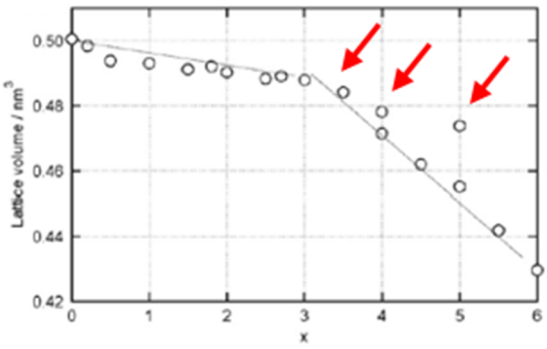

FIG. 6. The volumes of $Li_3InBr_{6-x}Cl_x$ at 500 K [Reproduced with permission from Tomita *et al.*, Solid State Ionics **179**, 867–870 (2008). Copyright 2008 Elsevier B.V.].

$Li_3InBr_{6-x}Cl_x$ does not follow Vegard's Law,[24] which states that the lattice parameter of an alloy is the linear weighted average of the lattice parameters of the parent compounds. Instead there are two trends of volume versus alloying: a Br-rich trend and a Cl-rich trend (Fig. 6). The slope of the Cl-rich region is steep because substituting larger Br anions into the Cl sub-lattice causes the volume to increase significantly. In contrast, substituting a smaller Cl into the Br sub-lattice does not cause as much strain. The abrupt change in slope between the two regimes indicates that the system likely exhibits some phase separating tendency.

The hysteresis in volume upon Cl substitution (red arrows in Fig. 6) after the $x = 3$ composition[3,12,25] further suggests the presence of some phase separating tendency. Some of the Cl-rich compositions follow the Br-rich volume-trend, while other samples at the same composition follow the Cl-rich trend. Samples with two different volumes indicate different structures. X-ray diffraction further indicates a phase-separation at the $x = 3$ composition.[12]

Accordingly, we simulated Li diffusion within a NP supercell of Br_3 (structure in Fig. 1). Figure 2 shows that at 500 K, the NP at 4262 Å^3 has a higher D than the solid solutions of Br_4 and Br_3 at almost any volume (except for Br_3 at 4389 Å^3, which is an unphysical ~6% volume expansion). At 500 K, the NP has an order of magnitude higher diffusion than the solid solution and is 3× larger than $Li_3InBr_4Cl_2$. Thus, Br_3 with a nanophase microstructure reproduces the experimental trend in conductivity with alloying: Br_6, **Br_3**(**NP**), Br_4, and Cl_6 (from largest to smallest).[12] Note that we simulated the NP with a 4112 Å^3 volume at 700 K and it has higher diffusivity than the solid solution with the same volume (Table SI.1 of the supplementary material). Thus, we assume that the NP will also have a higher diffusivity than the solid solution with the small volume at 500 K.

We chose to simulate the NP at the medium volume at multiple temperatures because the volume is closer to the relaxed (zero pressure) Br_3 volume (see the supplementary material). More importantly, we want to identify the effect of the microstructure on frustration, and the medium volume solid solution Br_3 has the highest D_0.

By calculating the energy of relaxed supercells, we find that the NP has *essentially equal* energy as the solid solution (Table SI.1 of the supplementary material). Furthermore, the higher diffusivity of the NP microstructure results in a higher cation configurational entropy, which may further stabilize the system. These energy differences support phase separation in the experimental conductivity measurements. As discussed below, the NP material has higher diffusivity at low temperature for two reasons: the expanded volume of the Cl region leads to a higher Li concentration and even higher Li diffusion. Additionally, more Li-ions jump in the interface between the Br and Cl regions.

The expanded NP Cl-region (compared to the Cl_6 volume) enriches the Li concentration compared to the Br region. We calculate that the percentage of Li in the Cl-rich side, Π_{ave}(Cl-rich), is 8%–9% percentage points larger than the Br-rich side for the simulations at different volumes and temperatures (Table SI.5 of the supplementary material). A similar effect has been discussed in the context of other phase-separating superionic systems, including AgCl/AgI.[10,11] A more general

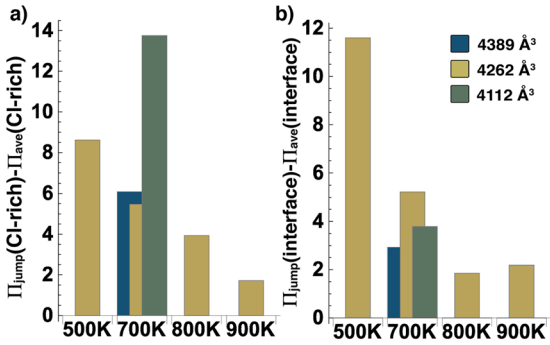

FIG. 7. (a) Π_i(Cl-rich) is the percentage of Li in the NP's Cl-rich region. Π_{jump}(Cl-rich) − Π_{ave}(Cl-rich) > 0 shows that more jumping Li ions are in the Cl-rich region. (b) Π_i(interface) is the percentage of Li in the interface between the Cl and Br rich regions. Jumping Li ions are more likely to be in the interface than the bulk.

theoretical formalism has also been suggested to describe the enrichment of the mobile ion species in terms of space-charge layer formation at a solid interface.[10,11,26–28] Our analyses at varying temperatures show that the expansion and compression of the Cl and Br regions change E_a and increase or decrease jump events, respectively.

Beyond Li enrichment, Li ions are also more likely to jump in the Cl-rich side; Π_{jump}(Cl-rich) is greater than Π_{ave}(Cl-rich). Figure 5(a) shows Π_{jump}(Cl-rich) − Π_{ave}(Cl-rich) > 0 for all simulations (see also Table SI.5 of the supplementary material). More Li ions jump on the Cl-rich side at small volumes (green > yellow) and lower temperatures. The increase in diffusion in the Br region as the temperature increases supports the hypothesis that E_a is larger in the Br region.

The interface between the Cl-rich and Br-rich regions (the channel in Fig. 1) is also strained. The effects of variations in volume and bond chemistry can lead to frustration of the Li–Br bonds. In the center of the interface, Li has 3 Br and 3 Cl bonds, which is used to distinguish Li in the interface versus the bulk. The percentage of jumping Li in the interface Π_{jump}(interface) is always higher than the average percentage of Li in the interface, Π_{ave}(interface), as shown in Fig. 7(b). E_a in the interface/channel is lower than the bulk, so more jumping occurs at lower temperatures; as temperature increases, the likelihood of jumping in the interface decreases, as expected. Note that the intermediate volume has the largest Π_{jump}(interface) − Π_{ave}(interface), probably due to the ideal volume for frustrated polar-covalent bonds, similar to the solid solution shown in Fig. 5.

In conclusion, we show how bond frustration and phase separation affect diffusivity in halide alloys. Calculation of E_a and D_0 across varying Cl/Br compositions and volumes highlights the importance of a low E_a and a large D_0 for superionic conductivity. We find that a large D_0 can be understood through bond frustration; the effect of strain and chemistry can be controlled through alloying. The "ideal" Li-Br bond length to maximize frustration and thus the jump attempt frequency occurs in $Li_3InBr_3Cl_3$ at a slightly expanded (3%) volume due to competition between polar-covalent bonds with the Br in the octahedral site. Finally, we show that the experimental trend in the conductivity with alloying can be understood if $Li_3InBr_3Cl_3$ has a phase-separated microstructure rather than a solid solution. Phase separation has the effect of enriching the Li concentration in the Cl-rich region, creating a space charge layer similar to that proposed for other halide superionic conductors.[10,11,26–28] These insights into halide alloying will provide an important key to finding better and faster solid electrolytes.

See supplementary material for additional information on supercell volumes and energies, diffusion coefficients, octahedral and tetrahedral site sizes, polar-covalent character of bonds, nano-phase Li and jump locations, and geometry optimization.

The authors gratefully acknowledge funding from LLNL Laboratory Directed Research and Development Grant No. 15-ERD-022. A portion of this work was performed under the auspices of the U.S. Department of Energy by LLNL under Contract No. DE-AC52-07NA27344. Computing

resources were made available under the LLNL Institutional Computing Grand Challenge Program. Thanks to Shannon R. McCurdy for statistical advice. This study was partially supported by the National Science Foundation under Grant No. DMR-1710630.

[1] K. Shahi and J. B. Wagner, Jr., "Fast ion transport in silver halide solid solutions and multiphase systems," Appl. Phys. Lett. **37**(8), 757–759 (1980).
[2] R. Mercier, M. Tachez, J. P. Malugani, and G. Robert, "Effect of homovalent (I-, Br-) ion substitution on the ionic conductivity of $LiI_{1-x}Br_x$ systems," Solid State Ionics **15**(2), 109–112 (1985).
[3] Y. Tomita, A. Fuji-i, H. Ohki, K. Yamada, and T. Okuda, "New lithium ion conductor Li_3InBr_6 studied by ^{7}Li NMR," Chem. Lett. **27**, 223–224 (1998).
[4] H.-J. Deiseroth, S.-T. Kong, H. Eckert, J. Vannahme, C. Reiner, T. Zaiß, and M. Schlosser, "Li_6PS_5X: A class of crystalline Li-rich solids with an unusually high Li+ mobility," Angew. Chem., Int. Ed. **47**(4), 755–758 (2008).
[5] Y. Zhao and L. L. Daemen, "Superionic conductivity in lithium-rich anti-perovskites," J. Am. Chem. Soc. **134**(36), 15042–15047 (2012).
[6] J. Zhu, Y. Wang, S. Li, J. W. Howard, J. Neuefeind, Y. Ren, H. Wang, C. Liang, W. Yang, R. Zou, C. Jin, and Y. Zhao, "Sodium ion transport mechanisms in antiperovskite electrolytes Na_3OBr and Na_4OI_2: An *in situ* neutron diffraction study," Inorg. Chem. **55**(12), 5993–5998 (2016).
[7] A. C. Luntz, J. Voss, and K. Reuter, "Interfacial challenges in solid-state Li ion batteries," J. Phys. Chem. Lett. **6**(22), 4599–4604 (2015).
[8] Z. Deng, B. Radhakrishnan, and S. P. Ong, "Rational composition optimization of the lithium-rich $Li_3OCl_{1-x}Br_x$ anti-perovskite superionic conductors," Chem. Mater. **27**(10), 3749–3755 (2015).
[9] M. A. Kraft, S. P. Culver, M. Calderon, F. Böcher, T. Krauskopf, A. Senyshyn, C. Dietrich, A. Zevalkink, J. Janek, and W. G. Zeier, "Influence of lattice polarizability on the ionic conductivity in the lithium superionic argyrodites Li_6PS_5X (X = Cl, Br, I)," J. Am. Chem. Soc. **139**(31), 10909–10918 (2017).
[10] U. Lauer and J. Maier, "Conductivity enhancement and microstructure in AgCl/AgI composites," Solid State Ionics **51**(3-4), 209–213 (1992).
[11] U. Lauer and J. Maier, "Electrochemical analysis of anomalous conductivity effects in the AgCl/AgI two phase system," Ber. Bunsengesellschaft Phys. Chem. **96**(2), 111–119 (1992).
[12] Y. Tomita, H. Matsushita, K. Kobayashi, Y. Maeda, and K. Yamada, "Substitution effect of ionic conductivity in lithium ion conductor, $Li_3InBr_{6-x}Cl_x$," Solid State Ionics **179**, 867–870 (2008).
[13] N. Adelstein and B. C. Wood, "Role of dynamically frustrated bond disorder in a Li^+ superionic solid electrolyte," Chem. Mater. **28**(20), 7218–7231 (2016).
[14] M. Born and R. Oppenheimer, "Zur quantentheorie der molekeln," Ann. Phys. **389**(20), 457–484 (1927).
[15] P. Giannozzi, S. Baroni, N. Bonini, M. Calandra, R. Car, C. Cavazzoni, D. Ceresoli, G. L. Chiarotti, M. Cococcioni, I. Dabo, and A. Dal Corso, "QUANTUM ESPRESSO: A modular and open-source software project for quantum simulations of materials," J. Phys.: Condens. Matter **21**, 395502 (2009).
[16] D. Vanderbilt, "Soft self-consistent pseudopotentials in a generalized eigenvalue formalism," Phys. Rev. B **41**, 7892 (1990).
[17] J. P. Perdew, K. Burke, and M. Ernzerhof, "Generalized gradient approximation made simple," Phys. Rev. Lett. **77**, 3865 (1996).
[18] N. Marzari, A. A. Mostofi, J. R. Yates, I. Souza, and D. Vanderbilt, "Maximally localized Wannier functions: Theory and applications," Rev. Mod. Phys. **84**, 1419–1475 (2012).
[19] A. Yoshiasa, F. Kanamaru, and K. Koto, "Local structure of the superionic conducting α-AgI type $AgI_{1-x}Br_x$ solid-solution," Solid State Ionics **27**(4), 275–283 (1988).
[20] K. Fajans and G. Joos, "Molrefraktion von ionen und molekülen im lichte der atomstruktur," Z. Phys. **23**(1), 1–46 (1924).
[21] B. Kozinsky, S. A. Akhade, P. Hirel, A. Hashibon, C. Elsässer, P. Mehta, A. Logéat, and U. Eisele, "Effects of sublattice symmetry and frustration on ionic transport in garnet solid electrolytes," Phys. Rev. Lett. **116**, 055901 (2016).
[22] J. B. Varley, K. Kweon, P. Mehta, P. Shea, T. W. Heo, T. J. Udovic, V. Stavila, and B. C. Wood, "Understanding ionic conductivity trends in polyborane solid electrolytes from *ab initio* molecular dynamics," ACS Energy Lett. **2**(1), 250–255 (2017).
[23] K.E. Kweon, J. B. Varley, P. Shea, N. Adelstein, P. Mehta, T. W. Heo, T. J. Udovic, V. Stavila, and B. C. Wood, "Structural, chemical, and dynamical frustration: Origins of superionic conductivity in closo-borate solid electrolytes," Chem. Mater. **29**(21), 9142–9153 (2017).
[24] L. Vegard, "Die konstitution der mischkristalle und die raumfüllung der atome," Z. Phys. **5**(1), 17–26 (1921).
[25] Y. Tomita, K. Yamada, H. Ohki, and T. Okuda, "Structure and dynamics of Li_3InBr_6 and $NaInBr_4$ by means of nuclear magnetic resonance," Z. Naturforsch. A **53**, 466–472 (1998).
[26] C. E. Goodyer, J. S. Fish, J. D. Fehribach, R. O'Hayre, and A. L. Bunge, "Modeling space charge layer interaction and conductivity enhancement in nanoionic composites," Electrochim. Acta **56**(25), 9295–9302 (2011).
[27] P. Knauth, "Ionic conductor composites: Theory and materials," J. Electroceram. **5**(2), 111–125 (2000).
[28] J. Maier, "Defect chemistry at interfaces," Solid State Ionics **70-71**, 43–51 (1994).